Available online at www.sciencedirect.com
SCIENCE DIRECT®
Electrochimica Acta 50 (2005) 4674–4682
ELECTROCHIMICA Acta
www.elsevier.com/locate/electacta

Characterization and application of electrodeposited Pt, Pt/Pd, and Pd catalyst structures for direct formic acid micro fuel cells

R.S. Jayashree [a], J.S. Spendelow [a], J. Yeom [b], C. Rastogi [a], M.A. Shannon [b], P.J.A. Kenis [a,b,*]

[a] *Department of Chemical and Biomolecular Engineering, University of Illinois at Urbana Champaign, 600 S. Mathews Avenue, Urbana, IL 61801, USA*
[b] *Department of Mechanical and Industrial Engineering, University of Illinois at Urbana Champaign, 600 S. Mathews Avenue, Urbana, IL 61801, USA*

Received 29 December 2004; received in revised form 21 February 2005; accepted 27 February 2005
Available online 23 March 2005

Abstract

In this work, we study the preparation, structural characterization, and electrocatalytic analysis of robust Pt and Pd-containing catalyst structures for silicon-based formic acid micro fuel cells. The catalyst structures studied were prepared and incorporated into the silicon fuel cells by a post CMOS-compatible process of electrodeposition, as opposed to the more common introduction of nanoparticle-based catalyst by ink painting. Robust, high surface area, catalyst structures consisting of pure Pt, pure Pd, and Pt/Pd = 1:1 were obtained. In addition, Pt/Pd catalyst structures were obtained via spontaneous deposition on the electrodeposited pure Pt structure. The catalyst structures were characterized electrochemically using cyclic voltammetry and chronoamperometry. All Pd-containing catalyst structures facilitate formic acid oxidation at the lower potentials and deliver higher oxidation currents compared to pure Pt catalyst structures. Fuel cells of these catalyst structures show that pure Pd catalyst structures on the anode exhibit the highest peak power density, i.e. as high as 28.0 mW/cm^2. The MEMS compatible way of catalyst electrodeposition and integration presented here has yielded catalyst structures that are highly active towards formic acid oxidation and are sufficiently robust to be compatible with post-CMOS processing.

Keywords: Direct formic acid fuel cell; Pt/Pd catalysts; Spontaneous deposition; Micro fuel cell; Electrodeposition

1. Introduction

Micro fuel cells are emerging as promising high energy density power sources for portable applications [1]. Fuel cells are capable of delivering higher energy densities than the most competitive rechargeable batteries, like Li-ion and Ni–Cd. One of the key challenges for integration of high energy density fuel cells in miniature electronic applications is the development of fabrication procedures that are compatible with MEMS and/or post-CMOS processes. Along these lines, we have reported earlier on the successful fabrication of silicon-based fuel cell membrane electrode assemblies (MEAs) that efficiently integrate flow field channels, current collectors (Au), and catalysts, on a single chip [2]. However, several challenges still remain in developing robust catalyst structures that (i) are compatible with post-CMOS processing; (ii) have high surface area; (iii) exhibit sufficient catalytic activity towards the fuel used; and (iv) can withstand operation conditions including temperature changes, shock, and vibration. In this work, we study the preparation and performance of robust high-surface-area Pt and Pd-containing catalyst structures for silicon-based formic acid micro fuel cells that fulfill the first three and possibly also the fourth of the aforementioned requirements.

Methanol and formic acid are promising liquid fuels for micro fuel cells. Several miniaturized proton exchange membrane fuel cells (PEM-FC) running on methanol or on formic acid have been reported [3–7,8]. Kelley et al. were the first to report methanol/air miniaturized fuel cells fabricated using MEMS and microfabrication techniques [7]. While methanol has been a fuel of choice for PEM-FCs for several years, Rice et al. have recently shown the viability of formic acid in a cm-scale fuel cell [8]. Compared to methanol, formic acid

* Corresponding author. Tel.: +1 217 265 0523; fax: +1 217 333 5052.
E-mail address: kenis@uiuc.edu (P.J.A. Kenis).

0013-4686/$ – see front matter © 2005 Elsevier Ltd. All rights reserved.
doi:10.1016/j.electacta.2005.02.018

has faster room temperature kinetics and has less of a tendency to crossover, but the energy density of formic acid is only one-third that of methanol [9].

There are two proposed pathways for formic acid or methanol oxidation, namely the '*direct pathway*' and the '*CO pathway*'. In the '*CO pathway*', formic acid or methanol is oxidized to an intermediate like CO, which bonds strongly to the Pt surface and impedes the adsorption of fuel species (catalyst poisoning). For methanol electro-oxidation, CO poisoning is reduced by the use of Pt/Ru catalysts [10]. Formic acid oxidation on Pt surfaces occurs through both the '*direct pathway*' and the '*CO pathway*' [8,11–13]. Lu et al. have shown that formic acid oxidation typically proceeds through the preferred '*direct pathway*' on Pd-modified Pt surfaces [11], and the suppression of CO formation on Pd-modified Pt has been confirmed by FT-IR studies [14].

Generally, Pt and Pt-based metal nanoparticles with high surface areas are used as catalysts in PEM-FCs. These nanoparticles are typically painted onto the current collectors with an ink containing the nanoparticles as well as a certain percentage of Nafion solution to act as the binder upon evaporation of the solvent [15,16]. The presence of Nafion as a binder in catalyst inks provides good adhesion as well as good protonic conductivity, but hampers the electronic conductivity of the matrix. McGovern et al. reported a 13% decrease in surface area and a 40% decrease in oxidation current density resulting from inclusion of Nafion in Pt black nanoparticle-based inks [17]. This method of catalyst application thus inhibits the complete utilization of the catalyst. Alternatively, Pt-based metal catalysts can be applied to carbon-based high surface area supports via electrodeposition [7,18,19]. Here we obtain high surface area catalyst structures on smooth supports by electrodeposition at high deposition rates leading to rough deposits [20,21]. A key advantage of using electrodeposition as the catalyst deposition technique is its compatibility with MEMS and post-CMOS processing, enabling more straightforward integration of micro fuel cells in silicon-based microelectronic applications.

In this paper, we report on the preparation, structural characterization, and the electrochemical activity of electrodeposited dendritic Pt (pure Pt), spontaneously deposited Pd on dendritic Pt (Pt/Pd-SD), co-electrodeposited Pt/Pd (Pt/Pd = 1:1), and electrodeposited Pd (pure Pd) catalyst structures towards formic acid oxidation. The performance of silicon-based micro fuel cells equipped with these catalyst structures will also be studied and compared.

2. Experimental

2.1. Microfabrication of Si-MEA assemblies

Silicon-based membrane electrode assemblies (Si-MEAs) were prepared using standard microfabrication processes. A 100 mm N-doped double-sided polished Si-wafer (Silicon Quest, 500 μm thick, ⟨1 0 0⟩ oriented) was covered on the front side with a 1000 Å Au layer by dc magnetron sputtering (∼10^{-2} Torr of Ar background pressure). Subsequently, this Au layer, the eventual current collector, is further patterned into circular grids using a multistep procedure involving photolithography and liftoff, as reported previously [22]. In brief, the same side was then covered via spincoating with a polyimide layer (PMDA-ODA PI2808, HD Microsystem) that was further patterned and etched using deep reactive ion etching (Plasma-Therm SLR 770) from the top and the bottom to yield the 50-μm thick Si-grids with 100-μm square holes. Si-MEAs (Fig. 1) were prepared by bonding two Si-grids to a Nafion-112 membrane (Fuel Cell Scientific, Stoneham, MA) in a sandwich configuration. Bonding of two Si-grids to the Nafion membrane was achieved using a hot pressing method in an anodic bonder (EV, 501 series) at 120 °C and a pressure of ∼200 N/cm^2. A polyimide adhesion promoter (VM652, HD Microsystem) was employed to enhance the adhesion between the Nafion membrane and the PMDA-ODA-covered surface of the Si-grids. A detailed description of the fabrication of these Si-MEAs can be found elsewhere [2,22].

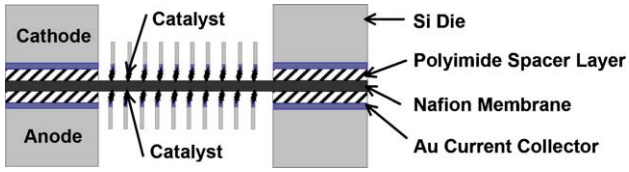

Fig. 1. Schematic diagram of micro fabricated Si-based MEA. In this paper, the cathode catalyst is always pure Pt, and the anode catalyst is pure Pt, Pt/Pd = 1:1, pure Pd, or Pt/Pd-SD.

2.2. Pt and Pt/Pd deposition

2.2.1. Pt deposition

High surface area, dendritic Pt catalyst structures (pure Pt) were prepared by electrodeposition on Au-coated Si-grids, either potentiostatically (−1, −2, or −5 V) versus a Ag/AgCl reference electrode (in 3 M NaCl, BAS, West-Lafayette, IN), or galvanostatically (−230, −1135, or −1365 mA/cm^2) in a 0.08 M $H_2PtCl_6{\cdot}6H_2O$ solution (Alfa Aesar) for 120 s, using an Autolab PGSTAT-30 potentiostat.

2.2.2. Spontaneous Pd deposition

The spontaneously deposited Pd on dendritic Pt (Pt/Pd-SD) sample was obtained by depositing Pd onto the high surface area dendritic Pt structures (pure Pt, Section 2.2.1) by spontaneous deposition as described elsewhere [11]. In short, the Pt-covered Si-MEAs were first cleaned electrochemically in 0.1 M H_2SO_4 (GFS Chemicals, Powell, OH) by cycling between 0 and 1.5 V versus RHE. Then the electrodes were placed in a 5 mM $Pd(NO_3)_2$ (Aldrich, 10 wt.% solution in 10 wt.% HNO_3) + 0.1 M H_2SO_4 solution for 5 min, followed by thorough rinsing with Milli-Q water (Barnsted E-pure water, 18 MΩ cm). These electrodes were electrochemically annealed by cycling five times between 0.05 and 0.95 V in 0.1 M

H_2SO_4. This spontaneous deposition procedure was repeated five times to yield Pd-decorated dendritic Pt catalyst structures (Pt/Pd-SD).

2.2.3. Co-deposition of Pt and Pd

Pt and Pd co-deposited catalyst structures (Pt/Pd = 1:1) were obtained by potentiostatic co-electrodeposition at −2 V versus Ag/AgCl for 120 s using a 0.04 M $H_2PtCl_6 \cdot 6H_2O$ + 0.04 M $PdCl_2$ (5 wt.% solution in 10 wt.% HCl solution, Aldrich).

2.2.4. Pure Pd deposition

High surface area Pd catalyst structures (pure Pd) were obtained by potentiostatic deposition at −2 V versus Ag/AgCl for 120 s using a 0.08 M $PdCl_2$ solution.

2.3. Surface area measurement of catalyst structures

The true surface areas of the Pt catalyst structures were determined from the hydrogen adsorption/desorption or CO stripping charge measured in 0.1 M H_2SO_4. The true surface areas of Pt/Pd and pure Pd catalysts were determined using CO stripping voltammetry. The geometric surface area of the Si-grids used to calculate current densities was 0.44 cm^2.

2.3.1. Hydrogen adsorption/desorption

Pure Pt catalyst structures were electrochemically cleaned in 0.1 M H_2SO_4 by cycling from 0.05 to 1.5 V versus RHE at a scan rate of 500 mV/s, followed by cycling in 0.1 M H_2SO_4 between 0.05 and 0.95 V versus RHE at a scan rate of 5 or 10 mV/s. The true surface area of the Pt catalyst was determined by calculating the charge associated with the hydrogen adsorption/desorption peaks using a charge to surface area value for hydrogen adsorption/desorption on polycrystalline Pt of 210 $\mu C/cm^2$ [23].

2.3.2. CO stripping

The Si-grids with Pd-containing catalyst structures were placed in 0.1 M H_2SO_4, and held at 0.1 V versus Ag/AgCl while the solution was bubbled with carbon monoxide gas (Matheson, 99.9% purity, Irving, TX) for 5 min. Then the solution was purged with N_2 (SJ Smith Welding supply, 99.9% purity, Davenport, IA) for 5 min to remove dissolved CO. Next, the electrodes were cycled between 0.05 and 1.2 V versus RHE, and the true surface areas of the catalyst structures were determined by calculating the charge corresponding to the CO stripping peak using a charge to surface area value for CO stripping on Pt or Pt/Pd of 420 $\mu C/cm^2$ [23].

2.4. Characterization of the catalyst structures

2.4.1. Morphology

The catalyst-covered Si-grids were mounted on conductive carbon tape for scanning electron microscopy (JEOL 6060LV microscope). High-resolution SEMs were obtained using a Hitachi S-4700 microscope.

2.4.2. Electrocatalytic analysis

Electro-oxidation of 0.1 M formic acid (Acros, 96%) in 0.1 M H_2SO_4 was studied using cyclic voltammetry and chronoamperometry.

2.4.2.1. Cyclic voltammetry. Electrochemically cleaned catalyst structures were cycled between 0.05 and 1.25 V versus RHE in 0.1 M H_2SO_4 + 0.1 M HCOOH solution at a scan rate of 10 mV/s.

2.4.2.2. Chronoamperometry. Potential steps between 0.95 and 0.01 V were applied for 1 s and these steps were repeated four times to ensure complete removal of surface-bound CO. After these cleaning steps the electrodes were held at 0.2, 0.3, or 0.4 V versus RHE for 600 s and the current was recorded as a function of time.

2.5. Pd quantification

2.5.1.1. Spontaneous deposition samples

After performing all electrochemical studies of formic acid electro-oxidation on Pt/Pd-SD, the catalyst structure was immersed in 1 mM NaI (Aldrich) for 5 min and then cycled in 1 M H_2SO_4 from 0.05 to 1.2 V versus RHE. The charge corresponding to the peak from 0.9 to 1.25 V due to anodic stripping of Pd and a charge to surface area value of 452 $\mu C/cm^2$ corresponded to a monolayer of Pd on Pt surface was used to calculate the number of Pd monolayers on the Pt surface [24].

2.5.1.2. Co-deposition samples

The atomic ratios of Pt and Pd in the co-deposited catalyst structures (Pt/Pd = 1:1) were determined during scanning electron microscopy (JEOL 6060LV SEM) with an energy dispersive X-ray analyzer (EDX, Oxford). The average composition of 15 different spots is reported. All measurements were within 10 at.% deviation from the average.

2.6. Fuel cell testing

The Si-grids with the desired catalyst (pure Pt, Pt/Pd = 1:1, Pt/Pd-SD, or pure Pd) as the anode, and a Si-grid with pure Pt deposited at −2 V versus Ag/AgCl for 120 s from 0.08 M $H_2PtCl_6 \cdot 6H_2O$ solution as the cathode were bonded to a Nafion-112 membrane in a sandwich configuration to obtain silicon-based membrane electrode assemblies (Si-MEAs) with different anode catalyst structures (see also Section 2.1). For testing, each Si-MEA was mounted on a test fixture as described earlier [22]. Fuel cell testing was performed by placing 2 ml of 10 M formic acid directly on the anode, and the cathode was exposed to a stream of oxygen at a flow rate of 10 sccm. The polarization curves were recorded by main-

taining a constant cell potential, and measuring the current in the circuit after waiting for the cell to reach steady state.

3. Results and discussion

3.1. Catalyst structure preparation on Si-grids

In previous work we reported on silicon-based membrane electrode assemblies (Si-MEAs, Fig. 1), comprised of two microfabricated Si-grids bonded to a Nafion-112 membrane [22]. In these Si-MEAs the flow-field, the current collector, and the catalyst structures are integrated on a single chip. Here, we integrate different catalyst structures on these Si-grids via electrodeposition. High surface area dendritic Pt catalyst structures (pure Pt) were obtained by electrodeposition on Au-covered Si-grids at different potentials and/or current densities (Table 1) to identify conditions yielding mechanically stable structures with high surface areas. Further studies were performed using the Pt catalyst structure deposited at −2 V, as the sample deposited at −5 V, while exhibiting a higher surface area, was mechanically unstable due to flaking. The co-deposited Pt/Pd catalyst structure (Pt/Pd = 1:1) and the Pd catalyst structure (pure Pd) were obtained by electrodeposition at −2 V from appropriate solutions (see Section 2.2). The Pt/Pd-SD catalyst structure was obtained by decorating pure Pt catalyst structures with Pd nanoislands by spontaneous deposition (see Section 2.2) [11].

3.2. Structural characterization of Pt, Pt/Pd, and Pd catalyst structures

The morphologies of the different catalyst structures were studied using scanning electron microscopy. Catalyst structures deposited at −1 V show a smooth morphology in SEM (Fig. 2a), while the catalyst structures deposited at −2 V exhibited a dendritic morphology (Fig. 2b and c). The catalyst structure deposited at −5 V exhibited dendritic morphol-

Table 1
Deposition conditions, surface areas, and current densities of Pt and Pd-containing catalyst structures

Catalyst structures	Deposition potential (V vs. Ag/AgCl)	True surface area[a] (m^2/g)	Current density ($\mu A/cm^2$)[b]		
			0.2 V vs. RHE	0.3 V vs. RHE	0.4 V vs. RHE
Pure Pt	−1	10.2	0.02	0.20	0.98
Pure Pt	−2	16.9	0.05	0.42	2.30
Pure Pt	−5	19.3	0.09	0.37	1.40
Pt/Pd = 1:1	−2	10.8	2.52	3.99	5.22
Pure Pd	−2	8.9	5.45	12.20	11.70
Pt/Pd-SD	−2	16.9	7.16	9.17	9.00

[a] Determined using cyclic voltammetry.
[b] Steady-state current densities (from chronoamperometry) in formic acid solution normalized to the true surface area of Pt catalyst structures.

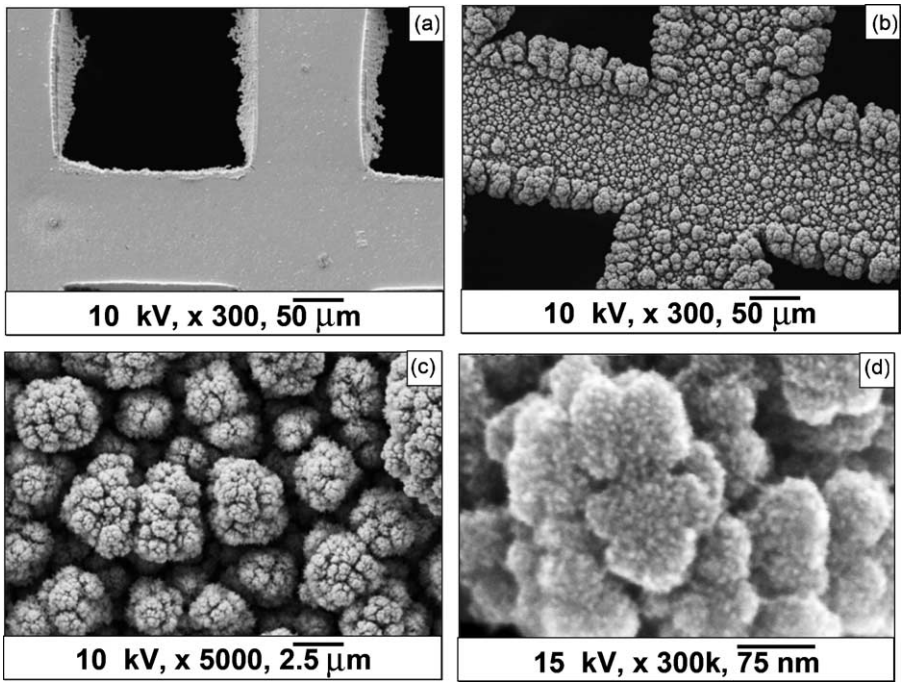

Fig. 2. Scanning electron micrographs of the pure Pt catalyst structures electrodeposited at (a) −1 V and (b–d) −2 V vs. Ag/AgCl, at different magnifications.

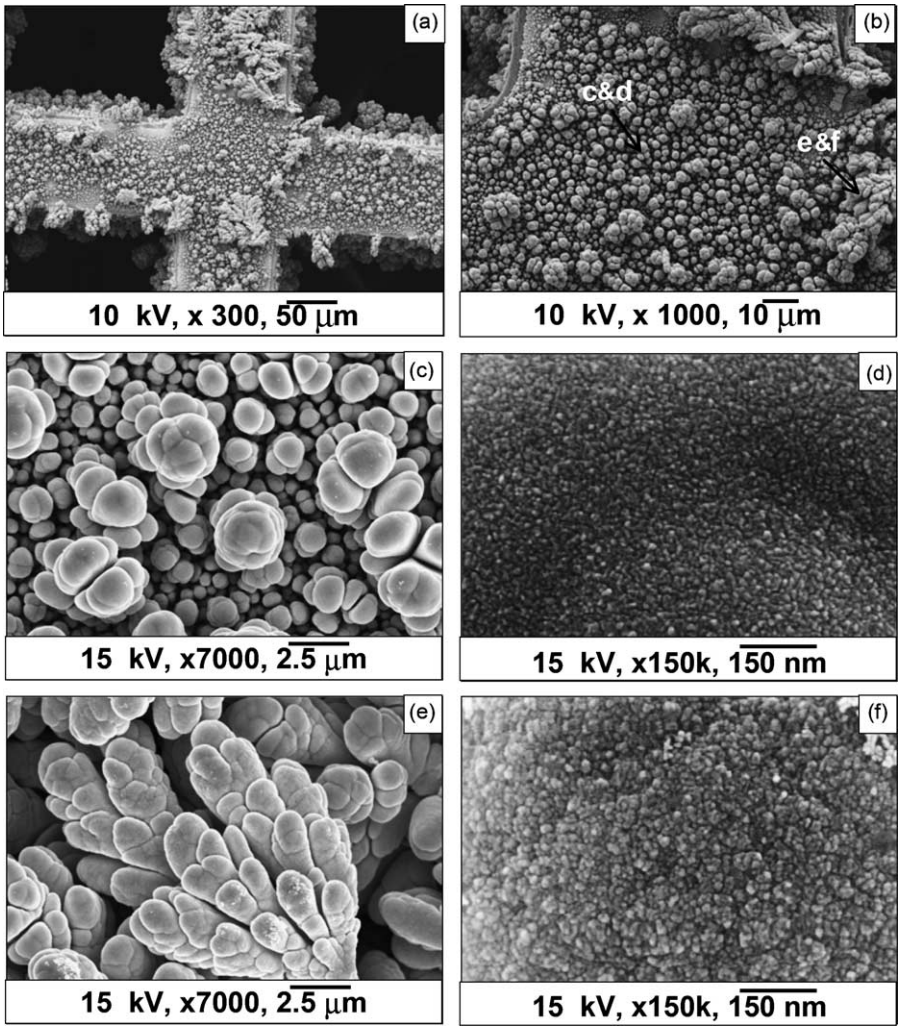

Fig. 3. Scanning electron micrographs of Pt/Pd = 1:1 catalyst structures codeposited at −2 V vs. Ag/AgCl at different magnifications. The existence of spherical, and wedge-shaped features can be seen in (b) and at higher magnification in (c and d) and (e and f).

ogy similar to catalyst structures deposited at −2 V. Such metallic dendritic morphologies obtained by high current or high potential electrodeposition have been reported by others [20,21]. We have used similar dendritic Pt structures as the catalysts in our previous work on Si-MEAs [22]. High-resolution images of dendritic Pt deposited at −2 V show the existence of nanopores (Fig. 2d). The presence of these nanoporous features explains the high surface area determined for these catalyst structures [18]. Using cyclic voltammetry, we measured surface areas increasing from 10.2 to 19.3 m^2/g for the pure Pt catalyst structures deposited at increasingly negative potentials (Table 1). This trend of increasing surface area corresponds to the increase in dendritic morphological character of the structures at increasingly negative potentials. Increasingly negative currents had a less pronounced effect; pure Pt catalyst structures deposited galvanostatically at −230, −1135, or −1365 mA/cm^2 resulted in surface areas of 16.6, 16.8, and 14.5 m^2/g, respectively.

SEM images of the Pt/Pd = 1:1 catalyst structure (Fig. 3) reveal the presence of spherical and dendritic features (Fig. 3b). High-resolution images indicate a granular nature of the spherical and dendritic particles (Fig. 3d and f). Energy Dispersive X-ray analysis (EDX) shows tht the ratio of Pt to Pd in this sample is 1:1. The surface area of co-deposited Pt/Pd = 1:1 was determined to be 10.8 m^2/g.

The pure Pd catalyst structures exhibit a variety of spherical features (Fig. 4). The surfaces of the larger spherical features that protrude further into the solution are made up of small (10–20 nm) round crystallites (Fig. 4d), while the smaller spherical entities in the recessed areas between them show fibrous surface features (Fig. 4c). These pure Pd have a surface area of 8.9 m^2/g.

The Pt/Pd-SD sample (not shown) did not exhibit any morphological differences compared to pure Pt samples (Fig. 2b), as expected. Using selective and quantitative anodic stripping of Pd, we determined that 0.23 monolayers of Pd islands were distributed on the Pt dendrites [24].

The difference in morphology of the pure Pt and the pure Pd catalyst structures is striking: The electrodeposition of pure Pt shows a nominal grain size of approximately 2.5 μm

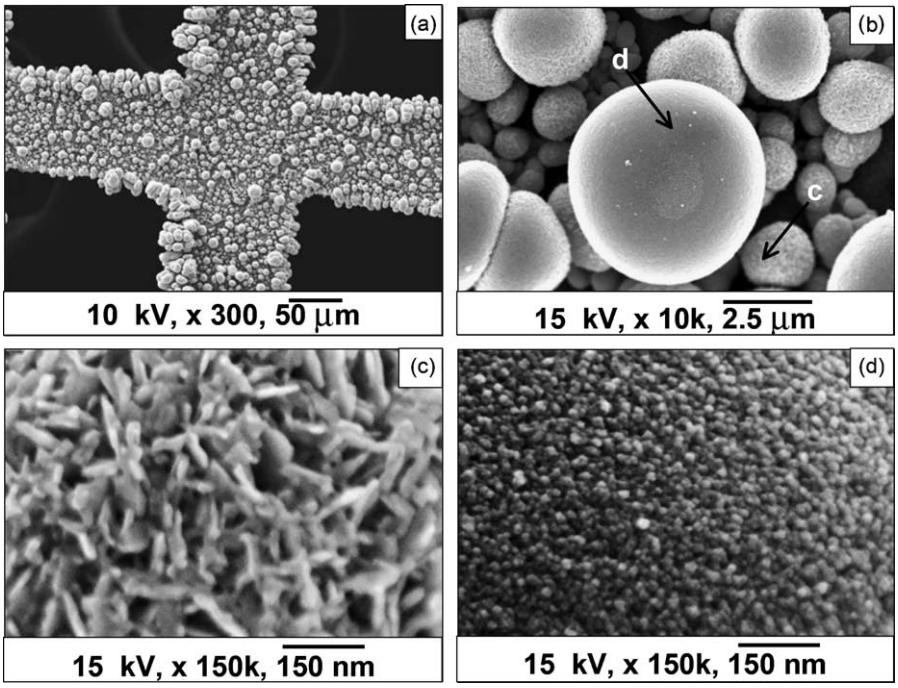

Fig. 4. Scanning electron micrographs of pure Pd catalyst electrodeposited at −2 V vs. Ag/AgCl. The existence of fibrous and smooth particles can be seen in (b) and at higher magnification in (c and d).

with a roughened surface with small granules of less than 100 nm, while the electrodeposition of pure Pd shows a larger variation of grain size ranging from less than 2.5 μm to more than 5 μm but all with a very smooth surface. At this point, we can only speculate about the origin of this difference, since the morphology of electrodeposited catalyst structures depends on a number of deposition parameters including the deposition potential and current densities (as studied for pure Pt), the duration, additives, and the chemical properties including differences in diffusivities, of the electrodeposited metal. Varying the potential and current we identified optimum deposition conditions for pure Pt of −2 V versus Ag/AgCl (Section 3.2). We used these conditions for the preparation of the other catalyst structures, including pure Pd. Explaining the origin of the different morphologies between the pure Pt and pure Pd catalyst structures and identifying critical parameters to control grain size for different catalysts would require further study of the deposition parameter space.

3.3. Electrocatalytic analysis

3.3.1. Cyclic voltammetry (CV)

Fig. 5 shows the forward (a) and reverse (b) scans of the four different catalyst structures of pure Pt, Pt/Pd-SD, Pt/Pd = 1:1, and pure Pd in a 0.1 M HCOOH + 0.1 M H_2SO_4 solution. For the pure Pt catalyst structures, the first anodic peak at 0.6 V corresponds to formic acid oxidation, while the second peak at 0.92 V can be attributed to CO oxidation and formic acid oxidation on sites that were previously blocked by CO. At higher potentials formic acid oxidation is deacti-

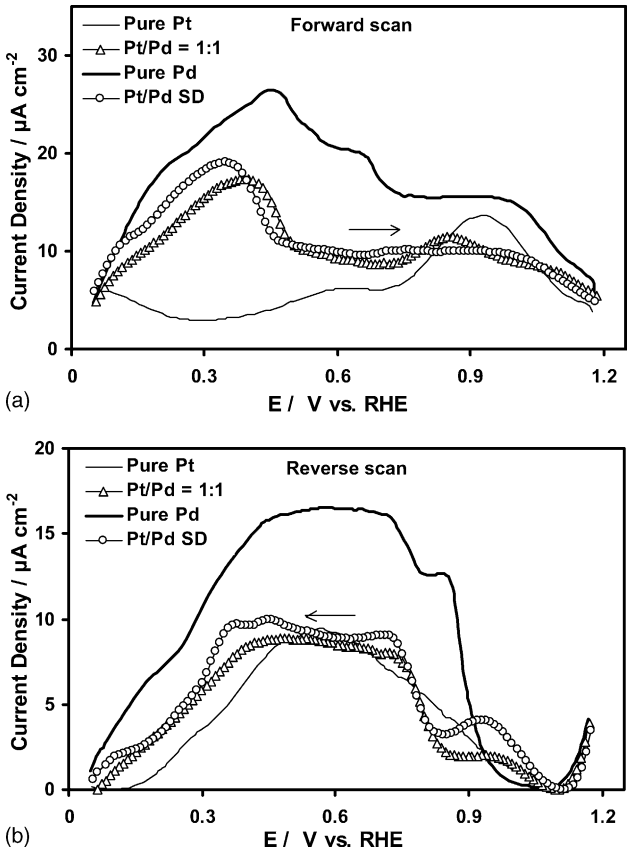

Fig. 5. (a) Forward and (b) reverse scans of cyclic voltammograms of pure Pt, Pt/Pd = 1:1, pure Pd, and Pt/Pd-SD catalyst structures in 0.1 M HCOOH + 0.1 M H_2SO_4. The current densities are normalized to the true surface area of the catalyst structures.

vated as a result of surface oxidation. The peak at 0.58 V in the reverse scan is due to the oxidation of formic acid after reduction of Pt oxides.

The formic acid oxidation peak shifts to lower values for the Pt/Pd = 1:1, Pure Pd, and Pt/Pd-SD samples compared to the pure Pt sample. This shift suggests that the Pt/Pd = 1:1, pure Pd, and Pt/Pd-SD catalyst structures exhibit better catalytic activity towards formic acid oxidation than pure Pt. The trends observed for the electrodeposited catalyst structures studied here are in agreement with previous formic acid electro-oxidation studies on nanoparticle-based catalysts [11].

3.3.2. Chronoamperometry (CA)

CA data of the pure Pt, Pt/Pd = 1:1, pure Pd and Pt/Pd-SD catalyst structures (Fig. 6a–c) were recorded by maintaining the electrode at a constant potential of 0.2, 0.3 or 0.4 V versus RHE in a solution containing 0.1 M HCOOH and 0.1 M H_2SO_4. At an applied potential of 0.2 V versus RHE (Fig. 6a), the Pt/Pd-SD sample exhibits the highest current density compared to the pure Pt, Pt/Pd = 1:1, and pure Pd samples. In this experiment, the current densities from the Pd-containing samples are about two orders of magnitude higher than the current density measured for the pure Pt catalyst structure at 0.2 V (Table 1). Moreover, at potentials of 0.3 and 0.4 V versus RHE, the pure Pd catalyst structure delivers a current density that is, respectively, 30 and five times larger than that for the pure Pt catalyst structure.

Formic acid oxidation can progress through two parallel pathways: a '*direct pathway*' in which formic acid is oxidized directly into CO_2 and a '*CO pathway*', which goes through the CO intermediate [11]. Higher potentials are necessary to oxidize the surface-bound CO, which leads to a decrease in cell potential in fuel cells [25]. In the case of Pd-containing catalyst structures, formic acid oxidation occurs on Pd sites through the '*direct pathway*', without the formation of surface-poisoning CO intermediates [11]. The chronoamperometric data of the Pd-containing catalyst structures studied here (Fig. 6) confirm the higher electroactivity towards formic acid oxidation: all Pd-containing catalyst structures exhibit higher steady-state currents than the pure Pt catalyst structures. The higher current densities from Pt/Pd-SD catalyst structures in comparison to Pt/Pd = 1:1 are most likely due to the random distribution of Pt and Pd atoms in the co-deposited Pt/Pd = 1:1 sample, whereas Pd nanoislands form on the Pt features in the Pt/Pd-SD catalyst structures [11]. On these Pd nanoislands formic acid oxidation occurs via the '*direct pathway*', leading to higher current densities.

An increase in current density in formic acid oxidation can be due to differences in catalyst composition as explained in the previous paragraphs. In addition, an increase in the surface area of the catalyst structures will lead to an increase in the current densities measured in chronoamperometry. For example, the steady-state current densities normalized to the true surface area for the different pure Pt structures (Table 1) increases as a result of the increase in surface area of catalyst structures deposited at increasingly negative potentials, −1 to −5 V.

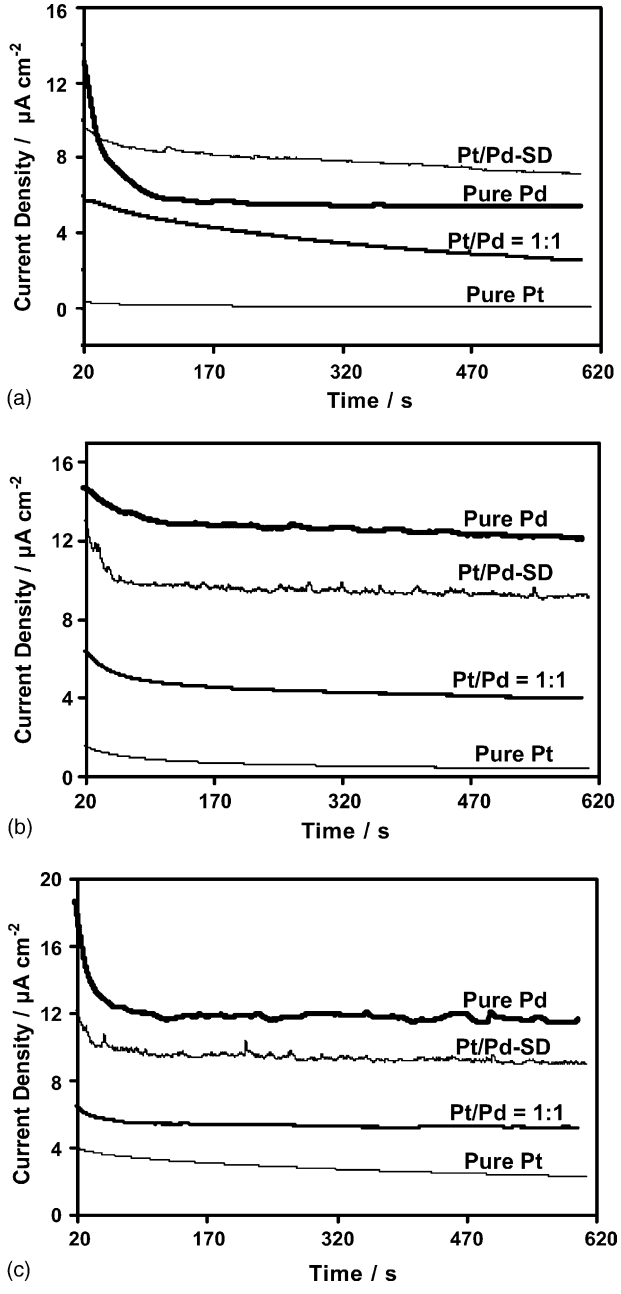

Fig. 6. Chronoamperometric data from pure Pt, Pt/Pd = 1:1, pure Pd, and Pt/Pd-SD catalyst structures studied at (a) 0.2 V, (b) 0.3 V, and (c) 0.4 V vs. RHE in 0.1 M HCOOH + 0.1 M H_2SO_4. The current densities are normalized to the true surface area of the catalyst structures.

3.4. Fuel cell testing

To test these catalyst structures in actual fuel cells, we assembled Si-MEAs (Fig. 1) comprised of Si-grids with pure Pt, Pt/Pd = 1:1, Pt/Pd-SD, and pure Pd catalyst structures on the anode side, and Si-grids with pure Pt catalyst structures

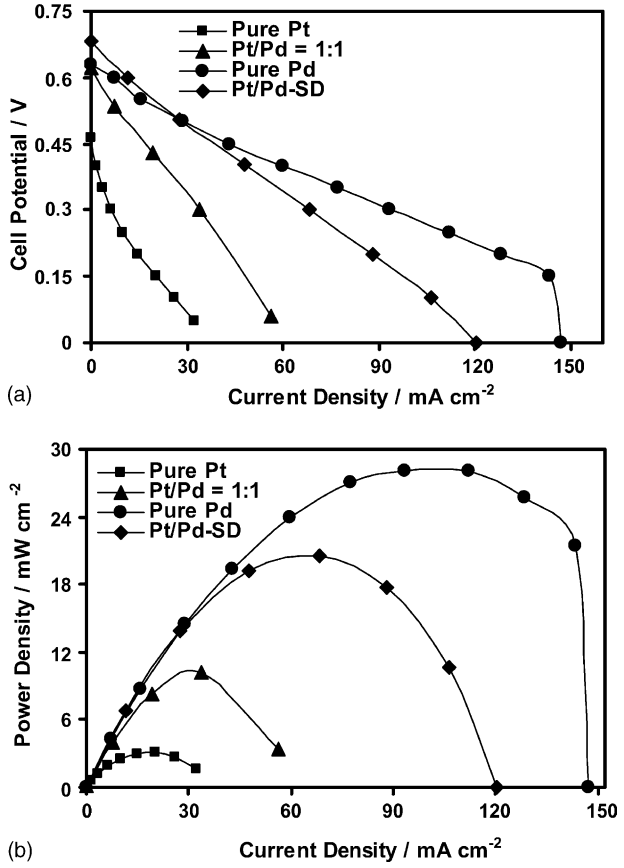

Fig. 7. (a) Polarization and (b) power density curves from Si-MEAs with pure Pt, Pt/Pd = 1:1, pure Pd, or Pt/Pd-SD catalyst structures as the anode, and pure Pt as the cathode. The current densities are normalized to the geometric surface area of the electrodes.

on the cathode side. The polarization and power density curves of these integrated Si-MEAs are shown in Fig. 7. The open circuit potentials (OCPs) of the Si-MEAs with pure Pt, Pt/Pd = 1:1, Pt/Pd-SD, and pure Pd, catalyst structures on the anode were 0.46, 0.62, 0.68, and 0.63 V, respectively, while the peak power densities were 3.0, 10.1, 20.6, and 28.0 mW/cm^2, respectively. At cell potentials $\geq$0.5 V, the Pt/Pd-SD sample exhibited the highest current density, which is in agreement with the results from CA, on the same sample at an applied electrode potential of 0.2 V versus RHE. Note that a lower applied potential in CA corresponds to a higher measured cell potential in fuel cell measurements. At cell potentials $\leq$0.5 V, the highest current densities were obtained from the Si-MEA with pure Pd catalyst structures at the anode.

Formic acid oxidation on pure Pt catalyst structures requires concomitant CO oxidation, which leads to an increase in anodic potential and thus a decrease in cell potential [25]. In contrast, formic acid oxidation on Pd-containing catalysts occurs on Pd sites through the '*direct pathway*' without the formation of any CO species, thus enabling formic acid oxidation to occur at lower anodic potentials and thus higher cell potentials, which is better for fuel cell performance. Again, these trends are all in full agreement with trends observed for fuel cells using nanoparticle-based catalysts [26,27].

4. Conclusions

High surface area Pt, Pd, and Pt/Pd catalyst structures were prepared by electrodeposition at large overpotentials, as well as through spontaneous deposition of Pd on pure Pt structures. The resulting structures provide high surface area electrocatalysts on microfabricated silicon substrates via MEMS compatible preparation methods. The activity of these catalyst structures for formic acid oxidation was studied using electrochemical techniques, and improved activity toward formic acid oxidation was observed as a result of increased surface areas and/or different chemical composition of the catalyst structures. Catalyst structures with dendritic as well as other high surface area morphologies exhibited increased activity for formic acid electro-oxidation due to their larger number of active sites. Similarly, Pd-containing catalysts were found to be significantly more active than the pure Pt catalyst structures. In chronoamperometry at low anode potentials (which corresponds to high cell potentials in a fuel cell), Pt structures modified by spontaneously deposited Pd (Pt/Pd-SD) were found to be the most active electrocatalysts, while pure Pd structures showed higher activity at higher anode potentials, i.e. at lower cell potentials. Pure Pd catalyst structures may thus be a good choice for fuel cells continuously operating under high load.

Parallel fuel cell testing studies using formic acid as the fuel confirmed that cells constructed with Pd anodes gave the highest power density, although at the highest fuel cell potentials the performance of cells containing Pt/Pd-SD anodes was superior. Note that the use of formic acid, rather than methanol, in these fuel cells has several advantages over direct methanol fuel cells, including faster anode kinetics and smaller amounts of crossover through the Nafion membrane. The lower tendency for crossover allows for fuel delivery at high concentration directly on the Si-MEA, which greatly simplifies the fuel cells design, reduces parasitic losses, and thus increases the attainable overall energy density.

The electrodeposited catalyst structures studied here exhibit power densities as high as 28.0 mW/cm^2 when using formic acid as the fuel on pure Pd catalyst structures. For comparison, others have reported microfabricated fuel cells using methanol as the fuel with power densities ranging from the μW/cm^2 level to 20 mW/cm^2 at $T < 30\,^{\circ}$C [3–7]. In addition, the intimate bonding of these catalyst structures on the silicon-based current collector grids as well as the dendritic, rigid morphology of the catalyst structures themselves, fulfills key compatibility requirements with respect to robustness for post-CMOS processing, as well as use for its intended application in miniature microelectronics. Further testing is needed to determine whether these silicon-based MEAs also will withstand temperature changes, shock, and vibration.

Acknowledgements

The authors thank DARPA for financial support under U.S. Air Force Grant F33615-01-C-2172. The scanning electron microscopy work was carried out in the Center for Microanalysis of Materials, University of Illinois, which is partially supported by the U.S. Department of Energy under grant DEFG02-91-ER45439. We acknowledge V. Petrova and J. Mabon for helpful discussions. JSS acknowledges support from a National Science Foundation Graduate Research Fellowship.

References

[1] W.Y. Sim, G.Y. Kim, S.S. Yang, IEEE MEMS (2001) 341.
[2] J. Yeom, G.Z. Mozsgai, A. Asthana, B.R. Flachsbart, P. Waszczuk, E.R. Choban, P.J.A. Kenis, M.A. Shannon, in: First International Conference on Fuel Cell Science, Engineering and Technology, Rochester, NY, USA, 21–23 April 2003, Fuel Cell Science, Eng. Technol. (2003) 267.
[3] G.Q. Lu, C.Y. Wang, T.J. Yen, X. Zhang, Electrochim. Acta 49 (2004) 821.
[4] J. Li, C. Moore, P.A. Kohl, J. Power Sources 138 (2004) 211.
[5] S. Motokawa, M. Mohamedi, T. Momma, S. Shoji, T. Osaka, Electrochem. Commun. 6 (2004) 562.
[6] T.J. Yen, N. Fang, X. Zhang, G.Q. Lu, C.Y. Wang, Appl. Phys. Lett. 83 (2003) 4056.
[7] S.C. Kelley, G.A. Deluga, W.H. Smyrl, Electrochem. Solid-State Lett. 3 (2000) 407.
[8] C. Rice, S. Ha, R.I. Masel, P. Waszczuk, A. Wieckowski, T. Barnard, J. Power Sources 111 (2002) 83.
[9] Y.W. Rhee, S.Y. Ha, R.I. Masel, J. Power Sources 117 (2003) 35.
[10] J. Munk, P.A. Christensen, A. Hamnett, E. Skou, J. Electroanal. Chem. 401 (1996) 215.
[11] G.-Q. Lu, A. Crown, A. Wieckowski, J. Phys. Chem. B 103 (1999) 9700.
[12] R. Parsons, T. VanderNoot, J. Electroanal. Chem. Interfacial Chem. 257 (1988) 9.
[13] X.H. Xia, T. Iwasita, J. Electrochem. Soc. 140 (1993) 2559.
[14] M. Arenz, V. Stamenkovic, T.J. Schmidt, K. Wandelt, P.N. Ross, N.M. Markovic, Phys. Chem. Chem. Phys. 5 (2003) 4242.
[15] M.S. Wilson, S. Gottesfeld, J. Electrochem. Soc. 139 (1992) 28.
[16] M.S. Wilson, S. Gottesfeld, J. Appl. Electrochem. 22 (1992) 1.
[17] M.S. McGovern, E.C. Garnett, C. Rice, R.I. Masel, A. Wieckowski, J. Power Sources 115 (2003) 35.
[18] T.L. Knutson, W.H. Smyrl, 206th Meeting of the Electrochemical Society, Honolulu, 3–8 October, 2004.
[19] S. Litster, G. McLean, J. Power Sources 130 (2004) 61.
[20] A.C. Hill, R.E. Patterson, J.P. Sefton, M.R. Columbia, Langmuir 15 (1999) 4005.
[21] B. Ilic, D. Czaplewski, P. Neuzil, T. Stanczyk, J. Blough, G.J. Maclay, J. Mater. Sci. 35 (2000) 3447.
[22] J. Yeom, G.Z. Mozsgai, B.R. Flachsbart, E.R. Choban, A. Asthana, M.A. Shannon, P.J.A. Kenis, Sens. Actuators B, in press.
[23] E. Yeager, J.O. Bockris, B.E. Conway, S. Sarangapani (Eds.), Comprehensive Treatise of Electrochemistry, Electrodics: Experimental Techniques, vol. 9, 1984.
[24] E.A. Lafferty, Y.G. Kim, M.P. Soriaga, Electrochim. Acta 44 (1998) 1031.
[25] T.R. Ralph, M.P. Hogarth, Platinum Met. Rev. 46 (2002) 117.
[26] Y. Zhu, Z. Khan, R.I. Masel, J. Power Sources 139 (2005) 15.
[27] C. Rice, S. Ha, R.I. Masel, A. Wieckowski, J. Power Sources 115 (2003) 229.